



# Processing Effects on the Formability of Extruded Flat Products of Magnesium Alloys

Maria Nienaber, Karl Ulrich Kainer, Dietmar Letzig and Jan Bohlen\*

Magnesium Innovation Centre (MagIC), Helmholtz-Zentrum Geesthacht, Geesthacht, Germany

The development of microstructure and texture during flat product extrusion of magnesium alloys differs significantly from those of rolled sheets. It has especially been shown that the range of microstructures and textures is broad in the case of extrusion which allows significant variations of the resulting textures. Three wrought magnesium–zinc alloys with texture modifying elements Nd (ZN10), Ca (ZX10), and Al (AZ31) have been used to extrude flat band profiles with varied processing parameters. This allowed a variation of grain sizes and textures of the extrudates. The impact on the mechanical properties and the forming behavior (Erichsen values IE) is revealed and discussed with respect to the microstructure and texture. It can be shown that a weak alignment of basal planes is preferred for enhanced formability over a distinct alignment of basal planes even if oriented preferentially for basal slip.

**Keywords:** magnesium alloys, sheets, extrusion, mechanical testing, stretch forming, Erichsen value

## OPEN ACCESS

### Edited by:

John L. Provis,  
University of Sheffield,  
United Kingdom

### Reviewed by:

Indranil Basu,  
ETH Zurich, Switzerland  
Mihriban Ozden Pekguleriyuz,  
McGill University, Canada

### \*Correspondence:

Jan Bohlen  
jan.bohlen@hzg.de

### Specialty section:

This article was submitted to  
Structural Materials,  
a section of the journal  
Frontiers in Materials

**Received:** 08 March 2019

**Accepted:** 25 September 2019

**Published:** 10 October 2019

### Citation:

Nienaber M, Kainer KU, Letzig D and  
Bohlen J (2019) Processing Effects on  
the Formability of Extruded Flat  
Products of Magnesium Alloys.  
*Front. Mater.* 6:253.  
doi: 10.3389/fmats.2019.00253

## INTRODUCTION

Making use of the full advantage of magnesium as a lightweight material also requires the production of larger thin-walled components such as sheets. However, the formability of magnesium alloys at room temperature is restricted due to their hexagonal lattice structure and the related limited number of available or easily activated slip systems (Mordike and Ebert, 2001; Beausir et al., 2009). The ability to form related parts includes the underlying manufacturing process of the sheet, e.g., rolling, as well as the sheet forming process. Conventional sheet rolling is carried out with high technical effort as the degrees of deformation per rolling pass need to remain low (Friedrich and Mordike, 2006). Processing of sheets via extrusion has also been described, which requires (and allows) a single high deformation processing step (Hsiang and Kuo, 2003; Bohlen et al., 2016, 2018a; Wang et al., 2016). This enables forming microstructures and textures that could not be produced by conventional production methods like casting or rolling (Gall et al., 2013).

Several earlier studies on the relationship between microstructure and mechanical or formability properties (Bohlen et al., 2007; Stutz et al., 2011; Suh et al., 2015) have highlighted that the formation of strong textures, i.e., with distinctly aligned basal planes parallel to the sheet plane, is one drawback for enhanced formability. Alloying with rare earth or calcium has been emphasized for texture weakening and for enhancing the formability during sheet rolling (Bohlen et al., 2007, 2015; Al-Samman and Li, 2011; Liu et al., 2016).

Typically, extruded magnesium alloys in the form of round bars develop a fiber texture with a pronounced prismatic  $\langle 10\bar{1}0 \rangle$  component parallel to the extrusion direction (ED)

(Dillamore and Roberts, 1965). Fully recrystallized materials also tend to develop a tilting component with a rotation of up to 30° around the *c*-axis of the lattice structure, thereby concentrating the orientations around the  $\langle 11\bar{2}0 \rangle$  pole intensity parallel to ED (Yi et al., 2010). In all cases, these textures represent a distinct preference for basal planes aligned parallel to ED. It has been shown that alloying magnesium with rare earth elements or Ca leads to distinct texture changes if the extruded profile is a round bar with a rotational symmetry around ED (Stanford and Barnett, 2008b; Stanford, 2010a). The resulting textures of these extruded alloys are also rather weak. In these cases a so-called “rare earth texture component” has been identified, often along with a  $\langle 11\bar{2}1 \rangle$  pole parallel to ED, thus tilting basal planes out of ED. Geometrically, an easier activation of basal slip during mechanical testing parallel to ED is then realized and an increase in the ductility of these materials enabled (Stanford and Barnett, 2008b; Zhou et al., 2013; Jiang et al., 2016). However, in the case of extrusion of flat profiles (without the rotational symmetry) also such alloys tend to form strong textures even if the alignment of basal planes may not preferentially be parallel to the sheet plane (Gall et al., 2013; Bohlen et al., 2018a). To give an example, extruded sheets from rare earth alloys ZE10 and ME21 in Bohlen et al. (2016) show strong textures, while extruded round bar counterparts of the same or comparable alloys showed weak textures (Bohlen et al., 2010; Nascimento et al., 2010). Flat bands (or sheets) with such strong textures can perform reasonably in deep-drawing cases or tensile testing but significantly lack formability in stretch forming cases.

In a recent work, possibilities for controlling the texture development during extrusion of flat bands (virtually representing sheets) have revealed the ability to significantly change the texture during extrusion as a result of the adjustment of the extrusion parameters (Bohlen et al., 2016). Based on an example of a magnesium alloy ZN10 (Mg+ 1 wt.% Zn+ 0.6 wt.% Nd) this corresponds directly to the dynamic recrystallization and grain growth behavior during extrusion. Especially, if the temperatures are very high during extrusion the rare earth specific texture development can even be overcome, resulting in a classical alignment of basal planes along the sheet plane. It is noteworthy, that the latter effect is also consistent with the texture development of rare earth containing round bar extrusions at high temperature (Stanford, 2010b). A similar effect like Nd on the texture development of extruded flat products has been shown for Ca-containing alloys, e.g., ZX10 (Mg+ 1 wt.%, Zn+ 0.2 wt.% Ca) in Bohlen et al. (2018b).

In this work, texture modification during direct extrusion and annealing of a flat band with different extrusion speed is investigated on two magnesium alloys with Nd (ZN10) and Ca (ZX10) in comparison to a classical benchmark magnesium alloy AZ31. It is suggested that the extrusion speed has a direct impact on the dynamic recrystallization behavior whereas annealing will cause static recrystallization. The differences in the microstructure and texture development are revealed and related to the mechanical properties from tensile tests as well as to the formability in biaxial Erichsen deepening tests.

**TABLE 1** | Chemical composition of the alloys in this study; values in wt.%; Mg balance.

Alloy	Al	Zn	Ca	Nd	Mn
AZ31	2.88	0.90			0.21
ZX10		0.94	0.15		
ZN10		0.98		0.57	

## MATERIALS AND METHODS

The chemical composition of the three magnesium alloys, AZ31, ZX10, and ZN10 has been measured by using spark emission spectroscopy (SPECTRO, SPECTROLAB M). Results are collected in **Table 1**. The alloys were prepared by using a modified gravity casting technique including directional solidification in a crucible. Details on this process can be found elsewhere (Elsayed et al., 2011). Billets were machined to a diameter of 49 mm to fit the 50 mm container of the extrusion press and to a length of 150 mm. Solid solution annealing of the cast billet was carried out for 16 h at 500°C (ZN10) and 16 h at 400°C (ZX10 and AZ31).

Extrusion experiments were carried out using a 2.5 MN automatic extrusion press of Müller Engineering (Müller Engineering GmbH & Co. KG, Todtenweis/Sand, Germany). The extruded bands have a width of 40 mm and a thickness of 2 mm, which corresponds to an extrusion ratio of 1:24.5. Processing temperatures were 300°C for AZ31 and ZX10 and 350°C for ZN10 in order to meet a reasonable range for material flow during extrusion. The extrusion speed (ram speed) was varied between 0.6 and 2.4 mm/s, respectively, which refers to rather low profile exit speeds of 0.9 or 3.5 m/min.

Additional annealing of the flat bands after extrusion for 10 min has been applied in order to track the microstructure development. AZ31 and ZX10 were heat treated at 400°C and ZN10 at 450°C. All bands were air-cooled after annealing.

The initial microstructure of all the materials were observed by light optical microscopy. The samples were polished with fine SiC papers (#800, #1200, and #2500), diamond suspension and OPS (oxide polishing suspension). The polished samples were etched for several seconds in standard picric acid solution of 20 ml H<sub>2</sub>O, 7 ml acetic acid, 200 ml Ethanol, and 6 g of picric acid (as reported in Kree et al., 2004). Orientation maps on polished longitudinal sections of the extruded profiles have been measured using electron backscatter diffraction (EBSD) in a scanning electron microscope (Zeiss Crossbeam 550 L) and corresponding software to reveal grain orientations and grain characteristics. The orientation data are used to visualize the texture of the measured surface section as well as fractions of the microstructure. The nature of different grains is separated by using a grain property of the orientation distribution, the grain orientation spread (GOS). In this approach a concept from earlier works (Bohlen et al., 2015, 2016; Basu and Al-Samman, 2019) is repeated, assuming that recrystallized grains as a result of a nucleation and growth mechanism due to dynamic recrystallization will exhibit a low variation of their orientation.

However, grains which did experience active slip glide typically will show a higher orientation spread. In this work a separation of both fractions, assumed to represent a recrystallized and an unrecrystallized fraction of the microstructure, is based on a constraint of  $GOS = 1^\circ$ . For texture measurements samples of the flat bands were ground to their midplane and polished. An X-ray diffractometer (PANalytical X'Pert PRO MRD) with Cu  $K\alpha$  radiation and a beam size of  $2 \times 1 \text{ mm}^2$  was employed to measure six pole figures up to a tilt angle of  $70^\circ$ . Normalized and background-corrected pole figures were completely recalculated from the orientation distribution function by using an open-source code MTEX (Bachmann et al., 2010). The recalculated (0002)- and (10 $\bar{1}$ 0)-pole figures are used in this study to reveal the texture of the samples.

The tensile properties of the extruded alloys were measured using dog-bone-shaped specimens with a gauge length of 24 mm and a width of 5 mm. Tensile tests were carried out on a universal tensile testing machine (Zwick Z050) at room temperature with a constant initial strain rate of  $10^{-3} \text{ s}^{-1}$  parallel to the extrusion direction. The stretch forming behavior was investigated by using Erichsen tests on full sections of the extruded bands with a lubricant (OKS 352) at room temperature. The punch radius was 10 mm and the forming rate (punch displacement) 5 mm/min.

## RESULT

**Table 2** collects extrusion forces at the beginning, during (the middle) and the end of the extrusion experiments. As a result of the direct extrusion process the detected force includes a fraction required for the material flow (according to the flow stress) as well as a fraction for the friction between the billet and the container wall. Therefore, the force will continuously decrease during the extrusion experiment when the area of friction decreases due to the decreasing length of the remaining billet. The changing of this force in the middle range of the extrusion, i.e., the range on the flat band where samples were taken from, is averaged and it is shown that the variation is small for all six experiments.

The peak force is associated with the beginning of the material flow during the extrusion experiment. In the case of AZ31 there is a visible increase of this force with the increase of the extrusion

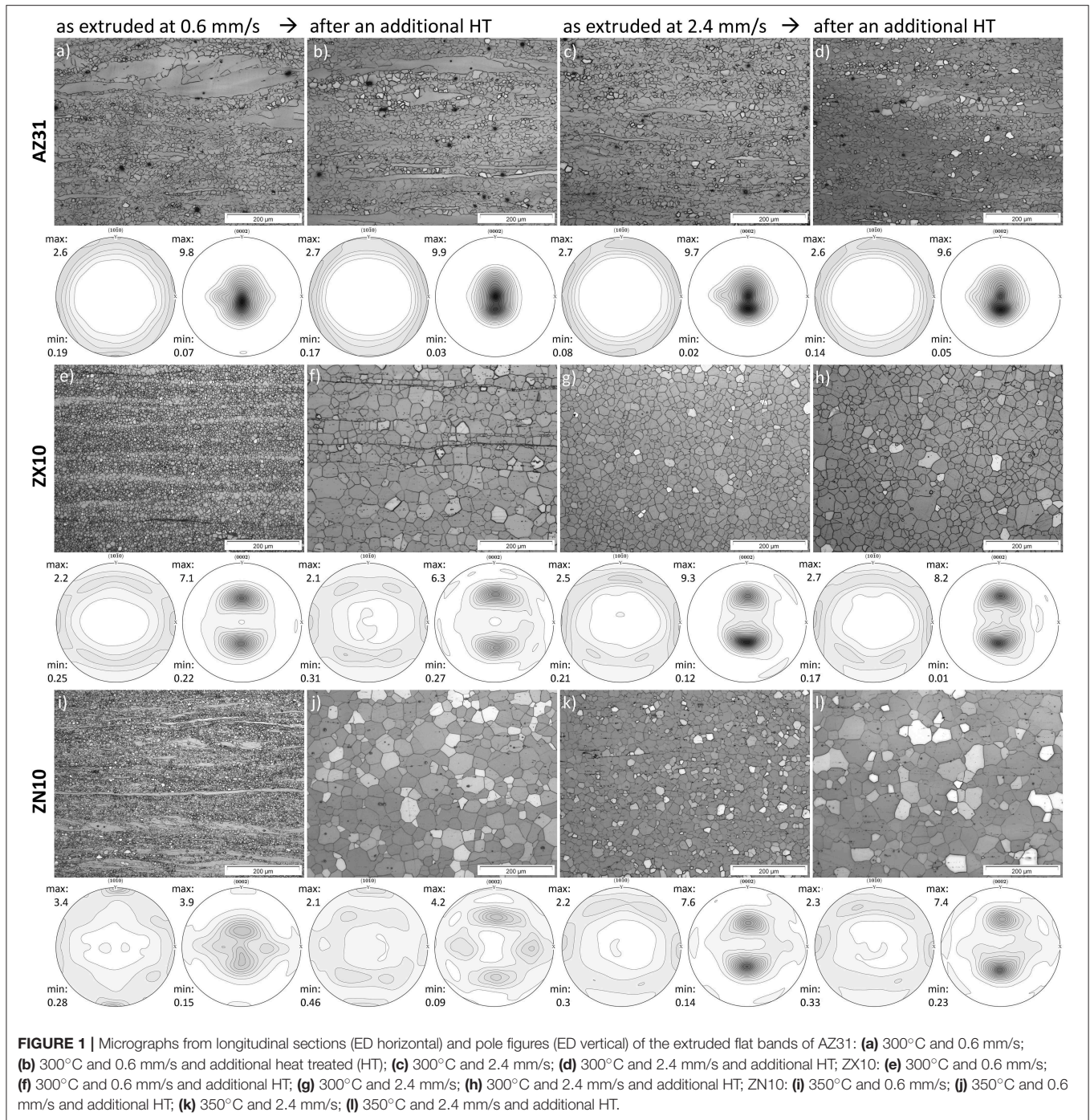
speed, indicating that higher force is required if the deformation rate is higher. During the experiment, the gap between the force levels decreases and vanishes at the end of the extrusion, thus indicating that there is no remaining difference in the force required for material flow (i.e., the flow stress will be the same). In the case of ZX10 and ZN10 the gap in the peak force does not even exist, indicating a low rate dependence of the flow stresses. Furthermore, at the end of the extrusion experiments, the forces will be even lower if the extrusion speed is higher. If only the higher deformation rate is considered, this finding appears counterintuitive, as higher strain rate would typically be associated with a higher flow stress (Atwell and Barnett, 2007; Liu et al., 2007). A deformation related heating of the sample is hypothesized which will also affect the microstructure development of the extrudates.

**Figure 1** shows the microstructure from the longitudinal section and the corresponding pole figures of the extruded bands. Resulting grain sizes are collected in **Table 3**. An increase of the extrusion speed leads to grain growth. The two as-extruded conditions of AZ31 (**Figures 1a,c**) are compared to their counterparts after annealing for 10 min at  $400^\circ\text{C}$  (**Figures 1b,d**). After slow extrusion with 0.6 mm/s (**Figure 1a**) a bimodal microstructure with non-recrystallized grains elongated parallel to extrusion direction (ED) is found. Fast extrusion with 2.4 mm/s (**Figure 1c**) qualitatively leads to an increase of the recrystallized fraction of the microstructure, however still maintaining elongated grains. The average grain size is  $9 \mu\text{m}$ . The annealing of both as-extruded conditions does not show a visible effect on the microstructure, which remains mostly unchanged compared to the as-extruded condition. Furthermore, the texture of the four conditions of AZ31 also does not vary much, maintaining a strong alignment of basal planes parallel to the band surface (i.e., c-axis parallel to the normal direction ND), and a broader angular tilt of basal planes to the extrusion direction rather than to the transverse direction. A tendency to develop split peaks between ND and a tilt toward the ED is visible after fast extrusion or after annealing. Prismatic planes are randomly distributed parallel to the ND of the flat band. The variation of the intensities is small. This texture results are typical for AZ31 and compare well to those of rolled or extruded sheets of this alloy (Styczynski et al., 2004; Yi et al., 2006; Victoria-Hernandez et al., 2014; Bohlen et al., 2018a).

ZX10 was extruded and annealed with the same conditions as AZ31. Microstructure and texture results are shown in **Figures 1e-h**. After slow extrusion at 0.6 mm/s, the microstructure is homogenous and almost completely recrystallized with a small grain size of  $4 \mu\text{m}$ . With fast extrusion at 2.4 mm/s, grain growth is observed, leading to an increase of the grain size to  $15 \mu\text{m}$ . Additionally, an influence of the heat treatment on the microstructure is shown in both initial states of ZX10, resulting in a distinct grain growth ( $23 \mu\text{m}$ ) after slow extrusion and a slightly lower grain size ( $21 \mu\text{m}$ ) after fast extrusion. Obviously, the annealing procedure dominates the microstructure development rather than the initial microstructure of the as-extruded condition of this alloy. The texture is fully different compared to AZ31 but the variations are

**TABLE 2** | Extrusion forces revealed from the extrusion experiments; peak force at the beginning of material flow (start of extrusion); force—middle of profile averaged from the center part of the profiles ranging over the part of the sample selection, and force—end of extrusion at the end of the extrusion experiment.

	Peak force (MN)	Force—middle of profile (MN)	Force—end of extrusion (MN)
AZ31 (0.6 mm/s @ $300^\circ\text{C}$ )	$1.86 \pm 0.01$	$1.15 \pm 0.06$	$0.90 \pm 0.01$
AZ31 (2.4 mm/s @ $300^\circ\text{C}$ )	$2.40 \pm 0.03$	$1.28 \pm 0.09$	$0.87 \pm 0.01$
ZX10 (0.6 mm/s @ $300^\circ\text{C}$ )	$2.57 \pm 0.01$	$1.56 \pm 0.07$	$1.20 \pm 0.01$
ZX10 (2.4 mm/s @ $300^\circ\text{C}$ )	$2.58 \pm 0.03$	$1.45 \pm 0.11$	$0.93 \pm 0.01$
ZN10 (0.6 mm/s @ $350^\circ\text{C}$ )	$1.93 \pm 0.01$	$1.39 \pm 0.07$	$1.06 \pm 0.01$
ZN10 (2.4 mm/s @ $350^\circ\text{C}$ )	$1.92 \pm 0.02$	$1.29 \pm 0.08$	$0.90 \pm 0.01$



also quite small. Split peaks of basal planes with a tilt toward ED are found. They are slightly more pronounced after fast extrusion but also weaken somewhat during annealing. Correspondingly, the prismatic planes are randomly distributed perpendicular to the two peak orientations of the basal poles, revealing a certain alignment parallel to ED (intensities at transverse direction TD) but no prismatic component or fiber in ED. This kind of texture of a calcium- or rare earth-containing Mg alloy has been described as a typical result for flat band extrusions and has

been associated with fully recrystallized microstructures of such samples (Bohlen et al., 2018b; Brokmeier, 2018).

ZN10 (**Figures 1i-l**) exhibits a partially recrystallized microstructure after slow extrusion with a distribution of very small grains embedded into elongated unrecrystallized grains. During heat treatment, significant grain growth is observed, leading to the coarsest grained microstructure of this study with an average grain size of 29 μm. After fast extrusion, the microstructure is completely recrystallized (12 μm) but during

**TABLE 3** | Grain size, Erichsen value (IE), and mechanical properties from tensile test in extrusion direction (ED) at room temperature of the extruded flat bands (TYS, tensile yield stress; UTS, ultimate tensile stress).

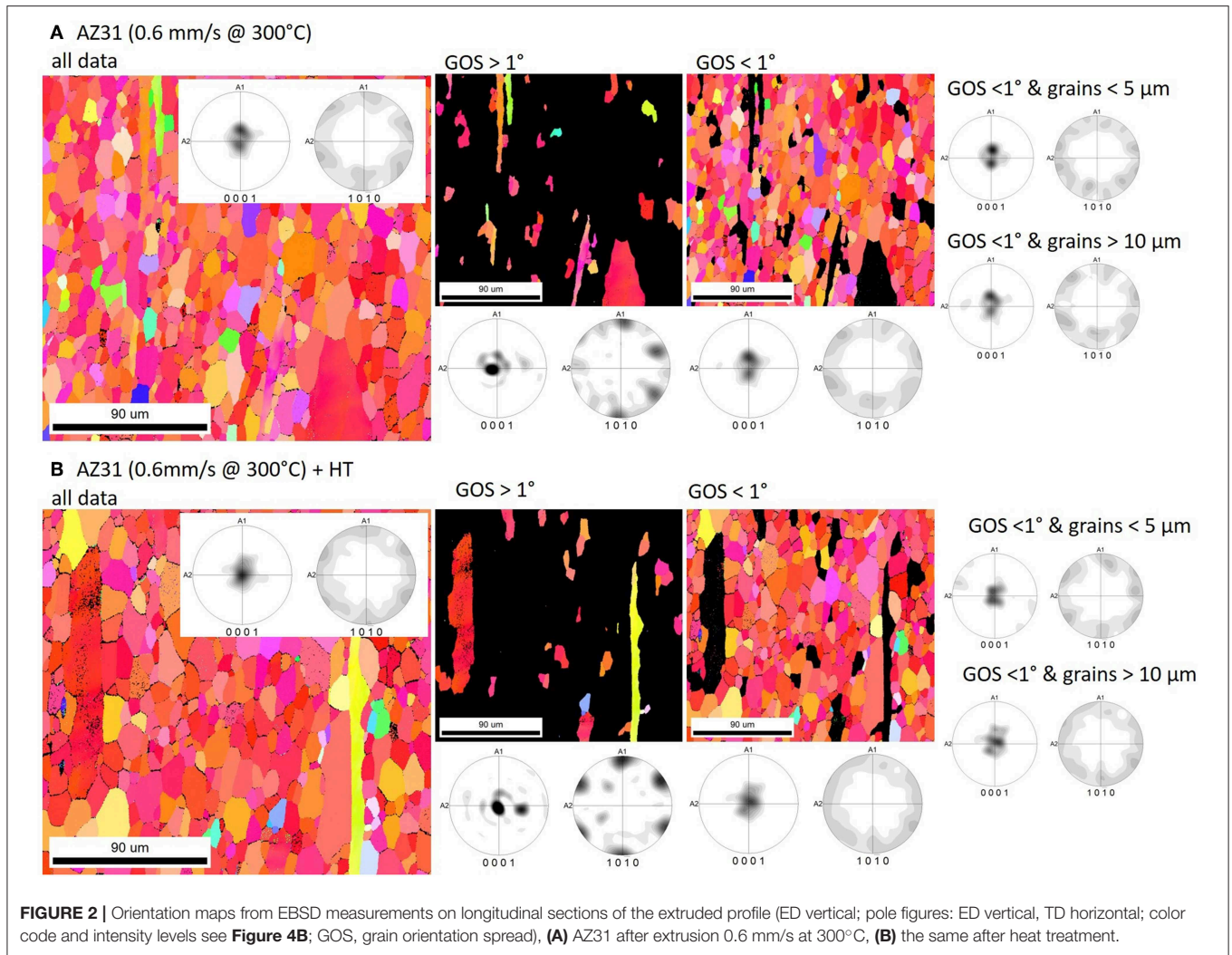
Alloy/condition	Grain Size ( $\mu\text{m}$ )	Erichsen value (mm)	TYS (MPa)	UTS (MPa)	Uniform strain (%)	Fracture strain (%)	$\Delta$ Stress = UTS-TYS (MPa)
AZ31 (0.6 mm/s @ 300°C)	6.7 $\pm$ 0.1	2.8 $\pm$ 0.2	151 $\pm$ 7	265 $\pm$ 2	18.6 $\pm$ 0.3	26.5 $\pm$ 0.1	<b>114</b>
AZ31 (0.6 mm/s @ 300°C) + HT	9.0 $\pm$ 0.7	2.8 $\pm$ 0.1	144 $\pm$ 2	256 $\pm$ 4	19.9 $\pm$ 1.1	26.5 $\pm$ 0.5	112
AZ31 (2.4 mm/s @ 300°C)	9.3 $\pm$ 0.5	2.8 $\pm$ 0.1	144 $\pm$ 6	257 $\pm$ 2	18.7 $\pm$ 1.1	25.8 $\pm$ 2.1	113
AZ31 (2.4 mm/s @ 300°C) + HT	9.9 $\pm$ 0.4	3.0 $\pm$ 0.1	153 $\pm$ 10	265 $\pm$ 5	17.8 $\pm$ 1.0	25.0 $\pm$ 0.9	112
ZX10 (0.6 mm/s @ 300°C)	4.0 $\pm$ 0.1	4.9 $\pm$ 0.4	127 $\pm$ 5	213 $\pm$ 4	25.1 $\pm$ 0.5	37.7 $\pm$ 2.8	<b>86</b>
ZX10 (0.6 mm/s @ 300°C) + HT	22.6 $\pm$ 1.9	<b>6.1 <math>\pm</math> 0.1</b>	70 $\pm$ 3	190 $\pm$ 3	<b>27.8 <math>\pm</math> 0.6</b>	<b>39.1 <math>\pm</math> 2.1</b>	120
ZX10 (2.4 mm/s @ 300°C)	14.9 $\pm$ 0.2	5.3 $\pm$ 0.4	78 $\pm$ 4	195 $\pm$ 3	24.6 $\pm$ 0.4	31.8 $\pm$ 3.5	117
ZX10 (2.4 mm/s @ 300°C) + HT	20.7 $\pm$ 2.1	5.0 $\pm$ 0.2	62 $\pm$ 7	185 $\pm$ 8	25.3 $\pm$ 0.7	35.2 $\pm$ 1.4	123
ZN10 (0.6 mm/s @ 350°C)	3.5 $\pm$ 0.2	4.0 $\pm$ 0.3	188 $\pm$ 11	248 $\pm$ 4	14.2 $\pm$ 0.4	22.3 $\pm$ 2.2	<b>60</b>
ZN10 (0.6 mm/s @ 350°C) + HT	28.5 $\pm$ 3.3	<b>7.2 <math>\pm</math> 0.2</b>	75 $\pm$ 4	189 $\pm$ 4	<b>23.0 <math>\pm</math> 1.0</b>	<b>34.9 <math>\pm</math> 4.0</b>	114
ZN10 (2.4 mm/s @ 350°C)	12.1 $\pm$ 0.9	6.1 $\pm$ 0.3	100 $\pm$ 7	206 $\pm$ 5	21.2 $\pm$ 0.4	33.0 $\pm$ 2.7	106
ZN10 (2.4 mm/s @ 350°C) + HT	25.3 $\pm$ 1.2	5.6 $\pm$ 0.3	73 $\pm$ 5	197 $\pm$ 2	22.6 $\pm$ 1.1	32.1 $\pm$ 4.5	124

Some significant values are highlighted.

annealing grain coarsening is also found (25  $\mu\text{m}$ ). Although the microstructure development is generally very similar to ZX10, it appears that recrystallized grains remain smaller during extrusion, although the extrusion temperature was higher. Furthermore, the impact of the higher annealing temperature is rather small when the grain size development of ZN10 is compared to ZX10. The texture development has also many similar features, e.g., maintaining the split peaks of basal plane orientations and the distribution of prismatic planes. Especially after fast extrusion, the texture of ZN10 compares well to the same condition of ZX10. Only the maximum intensities are lower but remain unchanged during annealing. However, after slow extrusion the split peaks of basal planes remain very weak with maximum intensities of 4.2 m.r.d. and basal planes also exhibit a broader angular distribution toward TD. This transversal spread corresponds to a prismatic component in the (10 $\bar{1}$ 0) pole figure along with ED, which also leads to higher intensity. After the heat treatment, the prismatic component is still visible but the split peaks of basal planes with tilt to ED are stronger. Additionally (hypothetically as a result of the transversal spread of basal planes in the as-extruded condition), two weak split peaks with tilt to TD are visible. This difference of the texture development corresponds to the partly recrystallized nature of the ZN10 sample after slow extrusion.

EBSO orientation maps of the extruded profiles are collected in **Figures 2–4**. Exemplarily, results for AZ31 after slow extrusion as well as after the corresponding heat treatment are shown in **Figures 2A,B**. In the as-extruded condition (**Figure 2A**) a grain structure with a tendency in elongation along the extrusion direction (vertical) is visible, therefore repeating the finding in **Figure 1a**. The corresponding pole figures more clearly reveal an alignment of basal planes with the band plane but with a preferential tilt in the form of split peaks toward the ED. While this tilt is not clearly visible in the rather small fraction of the unrecrystallized grains (GOS > 1°), the recrystallized fraction

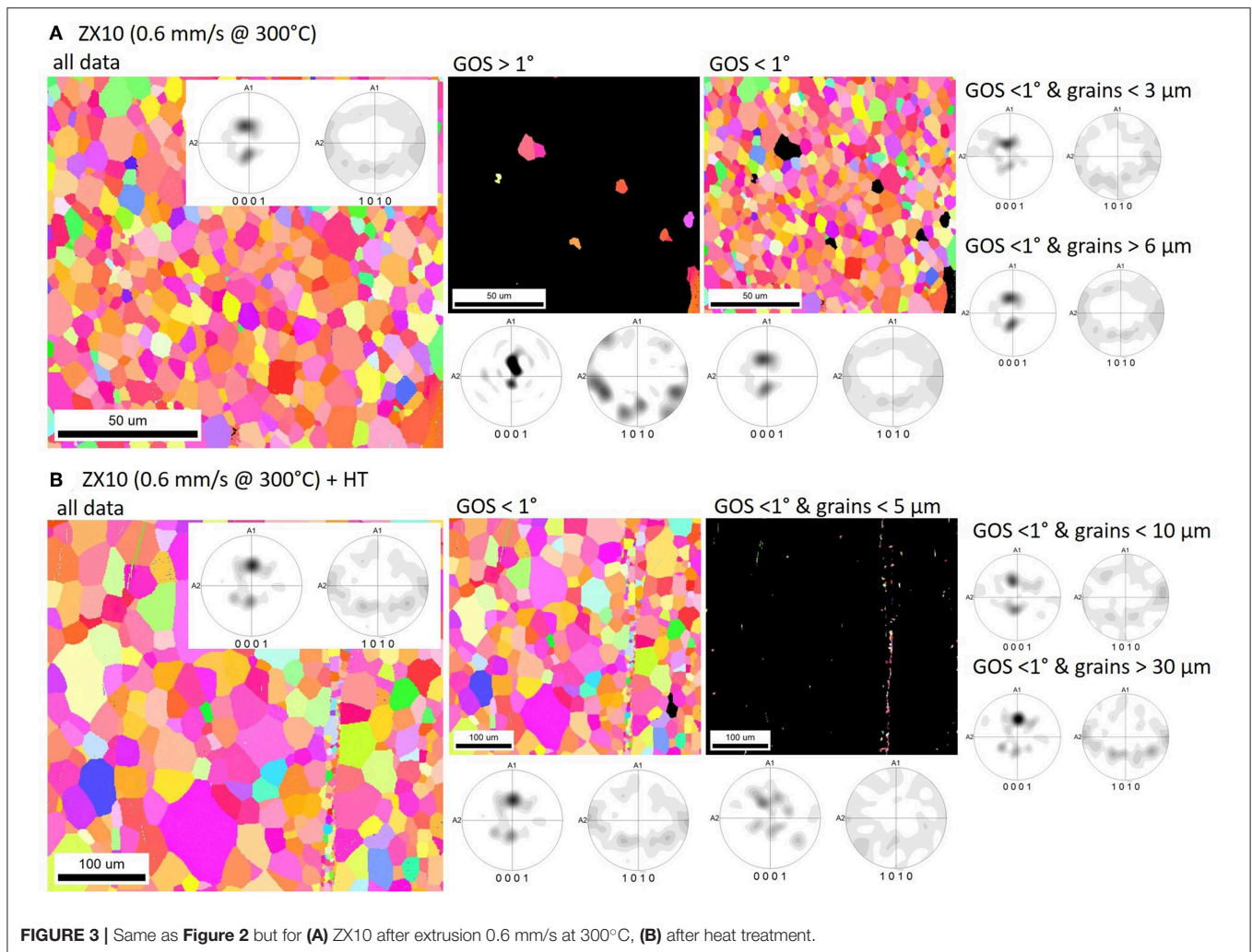
(GOS < 1°) is consistent with this finding. A separation of these recrystallized grains into smaller (e.g., <5  $\mu\text{m}$ ) and larger (e.g., >10  $\mu\text{m}$ ) fractions does not show any change and therefore no development tendency of orientations during grain growth. The heat treated counterpart in **Figure 2B** repeats these findings in a slightly coarser grained structure but with a stronger alignment of the basal planes, e.g., the split peaks are not visible any more in the (0001) pole figure. The separation into smaller and larger grains suggests a more visible basal alignment in the larger grains rather than in the smaller recrystallized grains, aiming toward a certain growth advantage of these grains and therefore strengthening the basal alignment. Such a behavior has often been reported for rolled sheets of AZ31 (Huang et al., 2012; Victoria-Hernandez et al., 2014). **Figures 3A,B** show the EBSO results for slowly extruded ZX10 and its heat treated counterpart, respectively. Even in the as-extruded condition the microstructure appears almost fully recrystallized, leaving only a few grains exceeding a GOS of 1°. While the overall texture repeats the extended basal split peak texture from **Figure 1e**, the few unrecrystallized grains appear again with a more distinct alignment along the surface of the extruded band. For the smaller and larger recrystallized grains, again no difference in the texture is found. In **Figure 3B** very similar findings are presented for a fully recrystallized microstructure and the same split peak texture. This texture again is confirmed for all distinguished grain size fractions from the smallest grains (e.g., in the extended band of very small grains) as well as in the very large grains of this sample. The significance of the split peak texture seems stronger in the larger grains, thus corresponding to a growth advantage. **Figure 4** compares the EBSO results for the four tested samples of alloy ZN10. The slowly as-extruded condition in **Figure 4A** reveals a distinct fraction of unrecrystallized microstructure. This high fraction exhibits a texture (see GOS > 1°) with split peaks toward the TD. Furthermore, a corresponding four peak alignment in the prismatic (10 $\bar{1}$ 0) pole figure together with



a strong prismatic peak in the ED is found. Obviously, an overemphasis of this fraction in the measured area leads to a clear difference of this texture compared to the one shown in **Figure 1i**. If only recrystallized grains are considered ( $GOS < 1^\circ$ ) the textures compare well, however, more distinctly showing the basal split peaks toward ED as well as a transverse spread including split peaks toward TD. A certain grain size tendency may be a higher significance of this component in the smaller recrystallized grains rather than in the larger ones. The prismatic component along ED is maintained at lower significance. The heat treatment of this sample, **Figure 4B**, allows maintaining both texture components with a certain emphasis of the ED split peak component in the larger grains. However, a clear TD spread component is not revealed any more in the fraction of the larger recrystallized grains. For the samples after fast extrusion and heat treatment, respectively, **Figures 4C,D**, again fully recrystallized microstructures are found with a possible strengthening of the ED split peak component in the larger grain fractions.

Stress-strain diagrams from tensile tests parallel to ED are shown in **Figure 5**. The corresponding mechanical properties

are collected in **Table 3**. In case of AZ31 only small variations can be seen. The yield stress (TYS) varies between 144 and 153 MPa. It slightly decreases with increasing extrusion speed but during annealing there is no clear tendency. The same is found for the maximum stress (UTS) between 256 and 265 MPa and the uniform elongation which averages at about 18.7% strain. The fracture strain is also comparable at 26%. Classical strain hardening with a continuous decrease of the slope is seen in the stress-strain diagrams. ZX10 reveals a much lower YYS (62–127 MPa) and UTS (185–213 MPa). After slow extrusion the lowest grain size corresponds to the highest stress levels followed by the fast extruded condition. The annealed samples with largest grain sizes also show the lowest stress levels. It is noteworthy that only the stress-strain-curve of the slowly extruded sample exhibits a flow instability at the yield point whereas all other conditions exhibit typical strain hardening behavior, obviously higher compared to AZ31. This also results in higher uniform strains as well as fracture strains. Both properties benefit from annealing but somewhat decrease with increasing extrusion speed.



Also for ZN10, the stress levels (TYS and UTS) correspond to the grain size of the samples. They are even higher in the as-extruded conditions compared to ZX10 but comparable in the annealed condition although grain sizes are larger. This indicates an advantage of ZN10 if initial higher stress levels are envisioned at comparable grain sizes. The curves indicate a special strain hardening behavior of the slowly as-extruded samples, which corresponds well to their partly recrystallized microstructure. The increase of stress during strain hardening remains low, which also corresponds to the lowest uniform strain and fracture strain in this study. Again, uniform strains and fracture strains benefit from the annealing after extrusion. However, both values remain lower in comparison to ZX10 (but higher than for AZ31).

The results from Erichsen cupping tests are collected in **Figure 6** in the form of exemplary drawing force—drawing path curves. The presented curves reveal the increase of the force after attaching the punch to the sample surface and the beginning of the deformation while forming the cup. The drawing path is then shown as the resulting depth of the formed cup. This force increase is continued until a sudden drop due to sample cracking. The respective force level does not vary much for the

four conditions of AZ31, it decreases only slightly with increasing extrusion speed but does not change due to the annealing of the samples. This finding is in good agreement to the strength considerations of this alloy as revealed from the tension tests. In the case of ZN10 and ZX10 the slowly as-extruded samples exhibit a steeper increase of the force levels compared to the other conditions, including the fast extruded samples as well as their annealed counterparts. This indicates principle strengthening of the samples as a result of the extrusion conditions. Consistently, the force levels of AZ31 remain higher than those of ZX10 and ZN10, although the maximum forces are lower due to early fracture of the samples.

The results from Erichsen cupping tests are collected in **Table 3** in the form of the Erichsen value (IE). This single value corresponds to the drawing length up to fracture of the samples, i.e., the depth of the formed cup as a result of biaxial stretching. For AZ31, the processing variations and the subsequent heat treatment show no influence on IE and remain at a very low level between 2.8 and 3.0 mm. This result compares well with the overall missing variation in the microstructure and texture development as well as with the tendency revealed for the

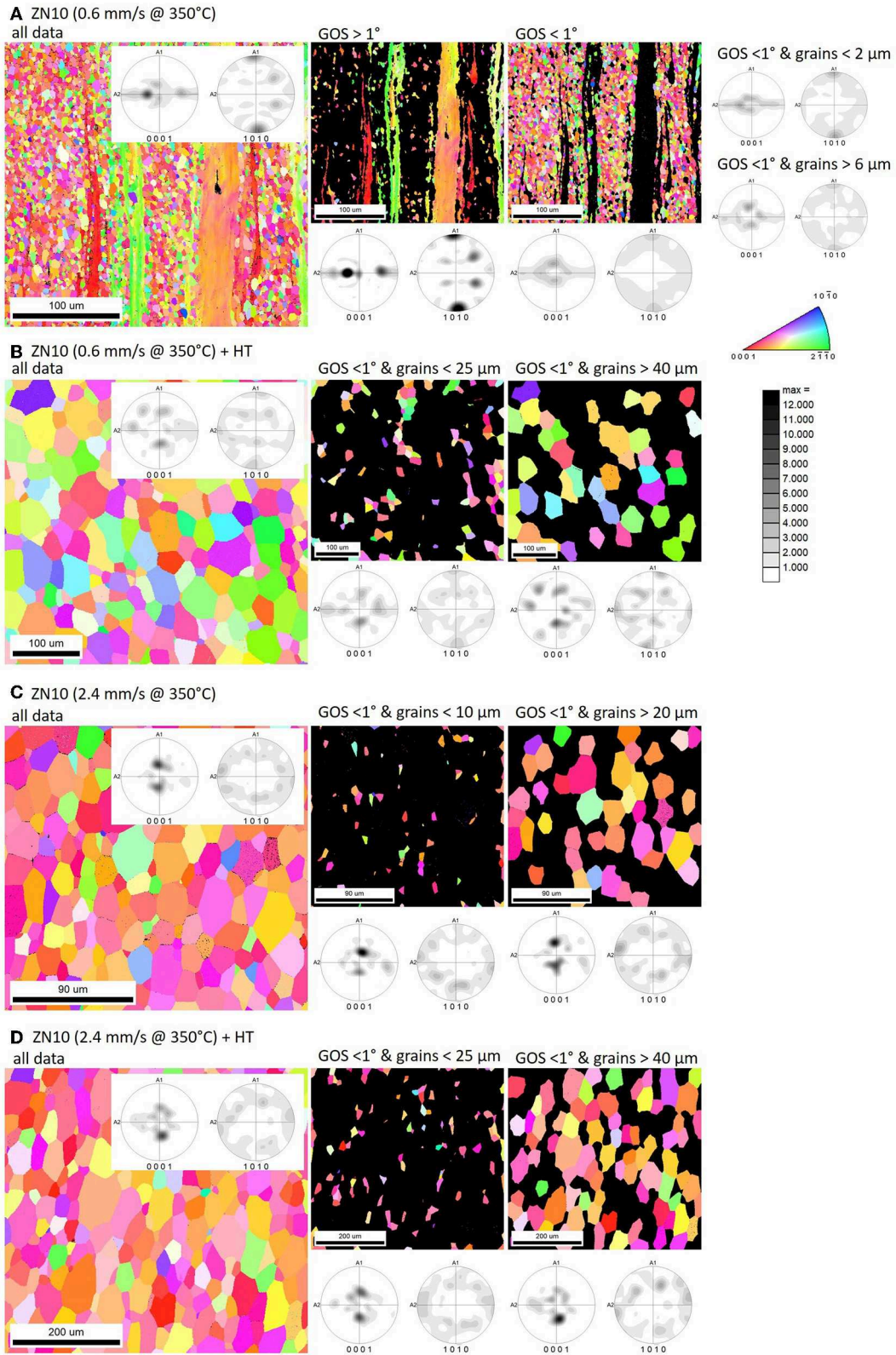
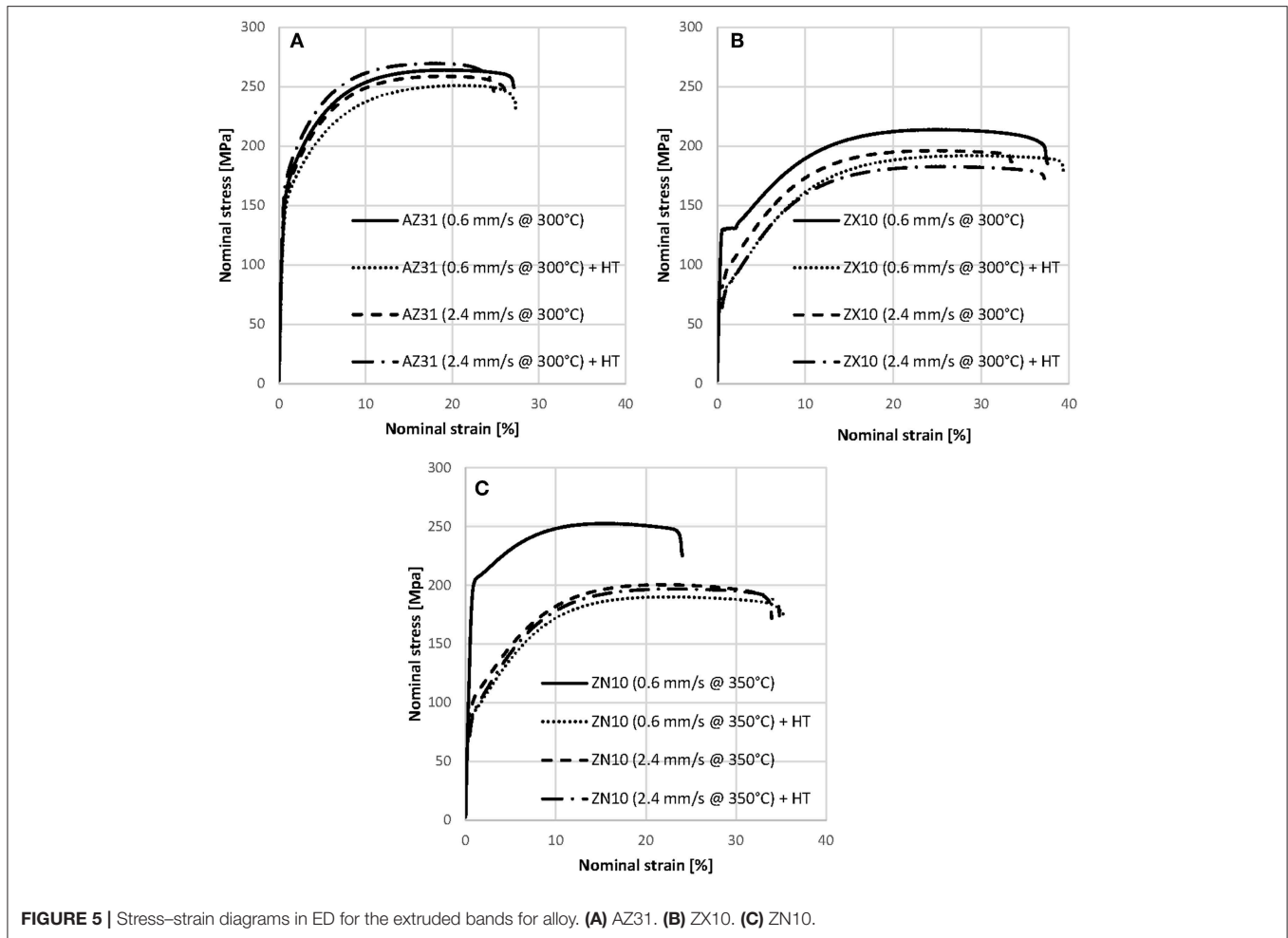


**FIGURE 4 |** Same as **Figure 2** but for **(A)** ZN10 after extrusion 0.6 mm/s at 350°C, **(B)** after heat treatment, **(C)** ZN10 after extrusion at 2.4 mm/s at 350°C, **(D)** after heat treatment.

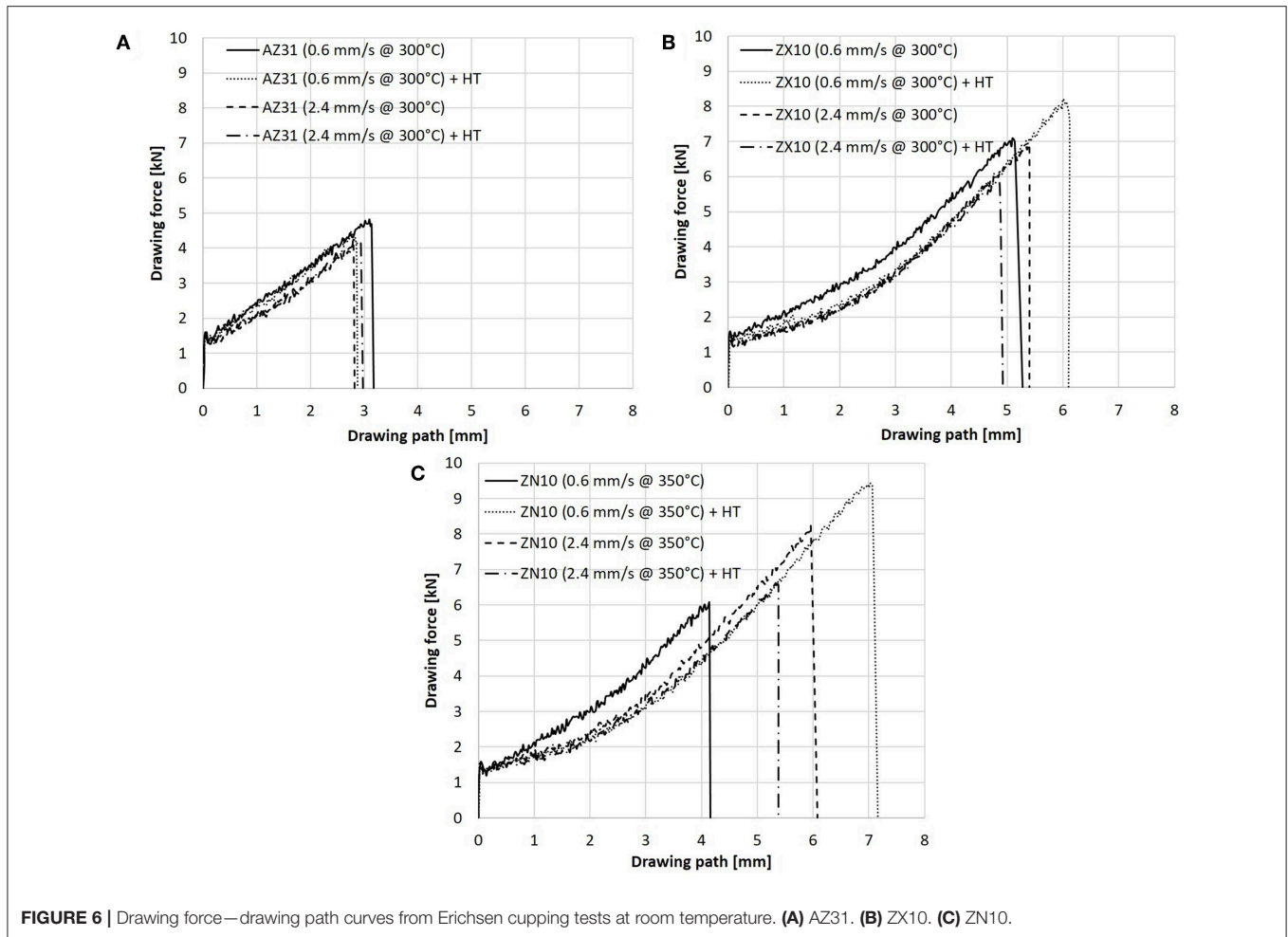


mechanical properties. ZX10 shows a clearly higher IE between 4.9 and 6.1 mm. The maximum value is found for the annealed condition after slow extrusion and corresponds to the highest strain properties of this alloy. Interestingly, this is not associated with a fine-grained microstructure but it corresponds to the weakest texture of this alloy, which does not vary much between the four investigated conditions. In case of ZN10, the variation of the IE is larger, varying between 4.0 and 7.2 mm. Again, the highest value is found for the annealed condition of the slowly extruded band at rather large grain size but also with the highest strain levels revealed for this alloy. With the exception of the partly recrystallized condition after slow extrusion the IE are higher for ZN10 compared to ZX10. Noteworthy, in case of the strain properties from tensile tests the finding was vice versa. However, in tendency this corresponds to slightly weaker textures of ZN10. Furthermore, especially after slow speed extrusion and its annealed counterpart the textures are very weak. Thus, the highest IE corresponds to a sample with a weak and broad orientation distribution of basal planes and a fully recrystallized (not necessarily fine-grained) microstructure. In summary, these Erichsen values are among the higher levels of state of the art magnesium alloy sheets (Chino et al., 2009; Lee et al., 2014; Wang et al., 2018).

## DISCUSSION

### Microstructure and Texture Development

High degrees of deformation for the extrusion of profiles lead to heating during the material flow through the die. Earlier works have reported on measurements of a deformation heating, which is also influenced by the applied extrusion speed (Liu et al., 2007; Yu et al., 2013). Thus, an increase of the extrusion speed (and corresponding strain rate) leads to a steady state temperature increase due to deformation heating. The resulting change in the flow stress will then have a direct impact on the extrusion force as measured at the end of the extrusion process where it is not superimposed by a friction component. A mechanism, which has a determining influence on the resulting flow stress (and extrusion force, respectively) is the dynamic recrystallization during forming. If the tendency to recrystallization is enhanced the flow stress/extrusion force will decrease. In this regards, the data from the extrusion forces in **Table 2** show a tendency of such a decrease with the increase of the extrusion speed, from AZ31 (−0.03 MN) to ZN10 (−0.16 MN) and to ZX10 (−0.27 MN). The same alloy tendency is found in the form of an increasing average grain size in **Table 3** for AZ31 (+2.6  $\mu\text{m}$ ) to ZN10 (+8.6  $\mu\text{m}$ ) and to ZX10 (+10.9  $\mu\text{m}$ ). A further comparison of the microstructure



development of the alloys does not seem appropriate as the initial extrusion temperatures needed to be varied for the different alloys in order to meet the extrusion windows. Still, the increase of the extrusion speed is associated with an enhancement of dynamic recrystallization and an alloy specific significance.

Furthermore, the resulting average grain sizes of ZN10 are lowest in this study at the highest initial billet temperatures, indicating a general retardation of recrystallization in this alloy compared to ZX10 or AZ31. The slowly extruded sample of ZN10 appears only partly recrystallized whereas both samples of ZX10 reveal fully recrystallized microstructures. For AZ31, the partly recrystallized microstructure still result in recrystallized grains grown much further than their ZN10-counterparts. This indicates a distinct difference in the recrystallization mechanisms. Such a difference has been investigated in related works, including an alloy specific change of the type of the dynamic recrystallization mechanism. A continuous type of recrystallization due to rearrangement and rotation of low angle grain boundaries toward high angle boundaries has been suggested instead of a dominating grain nucleation and growth mechanism (Barrett et al., 2017). Also particle stimulation of recrystallization is known as a specific mechanism of grain

structure formation (Ball and Prangnell, 1994; Al-Samman, 2013; Liu et al., 2018).

In order to understand the impact of recrystallization on the microstructure development it appears worthwhile to compare the textures of extruded round bars of magnesium alloys with those textures obtained from shaped flat profiles. Three important texture components of round bars can be repeated as follows: A strong prismatic fiber with high intensity in the  $(10\bar{1}0)$  pole figure along the ED has been associated with the remains of strong deformation textures in basically all magnesium alloy extrusions (Dillamore and Roberts, 1965; Stanford and Barnett, 2008b; Yi et al., 2010). A lattice rotation of up to  $30^\circ$  favors high intensity in the  $(11\bar{2}0)$  pole figure along ED for recrystallized extruded bars. A component exemplarily concentrating with high intensity in a  $(11\bar{2}1)$  pole figure is found in rare earth or Ca containing alloys, leading to a tilt of basal planes out of the ED. Retardation of recrystallization and corresponding new orientations developing as a result of deformation related orientation development include an impact of twins (Hantzsche et al., 2010; Al-Samman, 2013; Stanford, 2013; Minárik et al., 2019) and shear bands (Stanford and Barnett, 2008a; Zeng et al., 2019). Correspondingly, the textures of flat band extrusions

from various magnesium alloys have been described with respect to the specific shape given by the profile (Brokmeier, 2018). **Figure 7** collects sketches of such alloys representing the texture components of the samples of this study. **Figure 7A** shows a texture with an alignment of basal planes parallel to the band surface, also revealing high prismatic intensity in ED in the 6 peak symmetry of the prismatic pole figure. Note, that this texture is specifically expected if a deformation texture is hypothesized which is also visible from the texture of unrecrystallized grains ( $GOS > 1^\circ$ ) of AZ31 in **Figures 2A,B**. Basically the same alignment of basal planes is found in the recrystallized fraction of the microstructure but the six peak symmetry in the prismatic pole figure vanishes toward a rotational distribution of prismatic planes. This is the same reorientation as found in round bar extrusions as a result of recrystallization and the concurrent  $30^\circ$  reorientation of prismatic planes. The texture component in **Figure 7B** is based on two split peaks with tilt toward ED. It reveals an orientation which is not in accordance with prismatic pole intensity in ED but tilted. Note, that the recrystallized grain fractions in **Figures 3A,B** for ZX10 and in **Figures 4C,D** for ZN10 do not exactly match with this description but again better with a  $30^\circ$  rotation of the prismatic planes which makes this texture component well comparable to the “rare earth texture component” described for RE containing round bar extrusions. In conclusion this ED tilted basal split peak texture component is consistent with a modified rare earth texture component and its appearance in a profile without the rotational symmetry of a round bar is confirmed.

**Figure 7C** shows a component with two split peaks tilted toward TD. Correspondingly, a peak intensity in the prismatic pole figure along ED is visible. This component is very comparable to the one shown in **Figure 7A** if an additional TD tilt of the basal planes is acknowledged. It is only revealed for the partly recrystallized sample of ZN10 in this study, **Figure 4A**. Interestingly, the visibility of this specific orientation requires a shaped profile and cannot be distinguished for a round bar. In such a case it is consistent with a deformation related texture component, therefore in agreement with the unrecrystallized fraction of the microstructure for ZN10. Then the origin of this texture component requires an impact of different deformation mechanisms, especially other than in the case of AZ31. Although the specification of the nature of this effect is beyond the scope of this study, it has been shown that preferential prismatic slip instead of preferential basal slip is in accordance with such effects during sheet rolling (Styczyński et al., 2004).

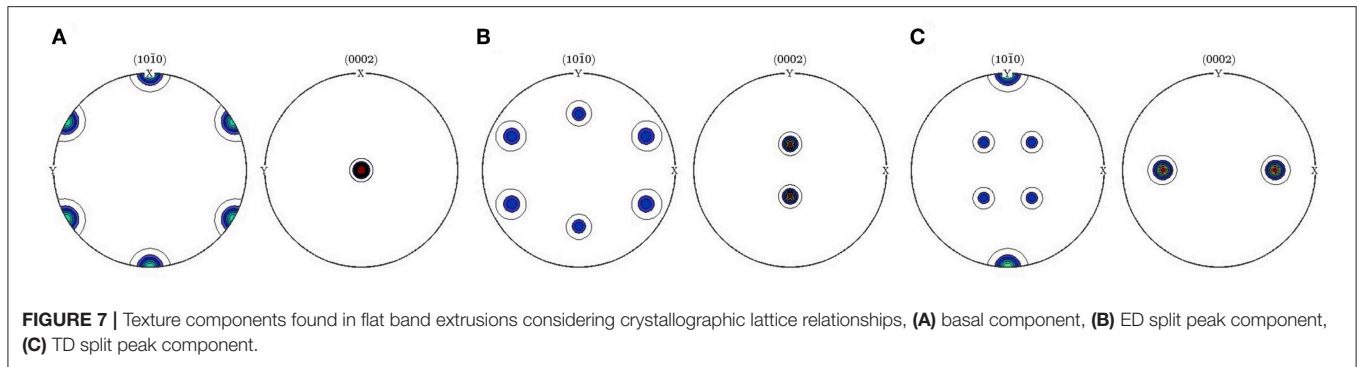
## Mechanical Properties and Formability

Experiments with two different strain paths were applied for the presentation of the mechanical behavior of the extruded bands. Tensile tests parallel to ED feature positive strain along the extrusion direction but corresponding free contraction along TD and ND. On the other hand, Erichsen cupping tests reveal the principal formability of the samples in operations with biaxial strain. In this condition, positive strain is enforced along ED and TD but contraction (thinning) is only freely enabled along ND. These two different procedures of plastic deformation are correlated to the microstructure and texture of

the materials of this study. Both tests are not expected to meet the same microstructure requirements for enhanced formability or ductility. In a simple consideration of dislocation driven deformation the ability of strain accommodation is related to the activity of the mechanism based on their activation (e.g., the critical resolved shear stress) as well as the orientation distribution of the respective lattice planes, i.e., described by the texture (Agnew et al., 2001; Bohlen et al., 2007; Hadorn et al., 2011; Miller et al., 2016; Chaudry et al., 2019). Thus, it appears worthwhile to concentrate on the contribution of basal slip with its low CRSS value and their orientation distribution (Chapuis and Driver, 2011; Wang et al., 2011; Kim et al., 2016; Liu et al., 2017) if texture effects are addressed, but not the initial effect of alloying elements on the ability of other (non-basal) slip modes to contribute to strain accommodation (Bohlen et al., 2007). In the case of a strong alignment of basal planes in the band plane like in AZ31 there is less ability for activation of basal slip in the uni-axial-tension case as well as in the stretch forming case. Therefore, stress properties remain comparably high and strain levels low as the strain hardening ability of the samples is limited. In cases with a tilt of basal planes toward ED slip activation is enhanced in the uni-axial case and the ability for strain accommodation increases. This is typically found for ZX10 and ZN10 in this study. Interestingly, the significance of such a component does not have a distinct effect on the strain accommodation. However, the yield stress remains lower in those cases if it is not also influenced by an unrecrystallized fraction of the microstructure which hypothetically can be assumed to be a harder fraction of the microstructure as a result of dislocation hardening during extrusion (e.g., slowly as-extruded conditions of ZX10 and ZN10), see discussion below.

In case of the biaxial test positive strain enforcement in all in-plane directions leaves material flow with negative strain along ND. Accommodation of such strain may require the same orientation considerations as above, but they are especially needed homogeneously in all in-plane directions. Although sample dimensions in this study did not allow revealing the mechanical behavior along the transverse direction, it has been shown in earlier work on extruded sheets that a strong anisotropy of the mechanical behavior is often correlated to limited stretch formability (Bohlen et al., 2018a). Forming limit curves revealed low formability in stretch forming conditions on the right side of the forming limit diagram but high formability on the left side, which in the context of this study compares to a strain path of the uni-axial tension test.

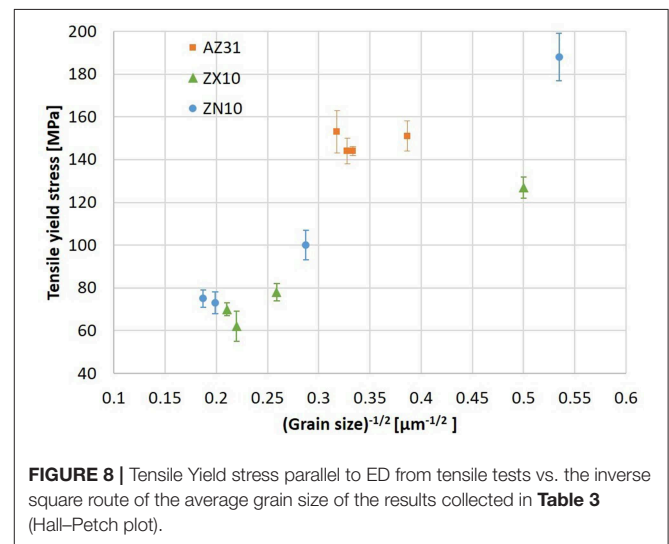
The split peak texture with tilt of basal planes appears to be beneficial for the strain properties in the tension test as well as for the stretch forming Erichsen cupping test and within each material a direct correlation can be found. Only in the case of ZN10 with especially weak distribution of basal planes and a concurrent further orientation component with tilt toward TD an additional increase of strain during the Erichsen cupping test is enabled. On the other hand, the weaker alignment of basal planes is not anymore beneficial for achieving very high uniform strains (and corresponding fracture strains) which leaves the strain levels of ZN10 lower compared to ZX10 as revealed from the tensile tests. This simple texture approach allows concluding



that weak textures with a more isotropic distribution of basal planes are required, especially to increase the stretch formability of magnesium sheets.

Such texture considerations do not include other microstructure related properties of the extruded and heat treated materials on the mechanical properties. Especially, the partly recrystallized microstructures may impose an impact on the strength properties of the samples, especially in the case of AZ31 and the slowly extruded ZN10. Together with the slowly extruded ZX10 (proven to be almost fully recrystallized in **Figure 3**) these samples exhibit high stress levels (TYS and UTS) compared to the fully recrystallized counterparts. Furthermore, if the ability to strain hardening is considered as the increase of stress from TYS to the UTS (**Table 3**) similar levels are found for AZ31 (~113 MPa) in accordance with the unchanged nature of the microstructure. In the case of ZX10 and ZN10, however, the lowest increase is clearly found for the slowly as-extruded samples, especially low for ZN10 (~60 MPa) with its clearly partly recrystallized microstructure. Although the quantitative fraction of the unrecrystallized microstructure cannot be directly resolved, the correlation of this strain hardening limitation to the degree of the recrystallized microstructure (and thus a partly strain hardened condition of the samples) becomes obvious. For the strain levels (uniform strain and fracture strain) this is directly confirmed for the partly recrystallized ZN10 after slow extrusion, not very distinct in case of ZX10 and again, not resolved for AZ31 based on the unchanged nature of the microstructures. Furthermore, it is also in agreement with the higher drawing forces required for Erichsen deepening in **Figure 6** as well as comparably lower Erichsen values, **Table 3**.

**Figure 8** shows the TYS plotted vs. the inverse square root of the average grain size (following the Hall–Petch relationship (Mann et al., 2004)). This plot has also been suggested in an earlier work (Stanford, 2013) to not only see the impact of grain boundary strengthening but also to visualize any deviation from the expected linear increase of TYS with the respective function of the grain size. In this plot, the above mentioned insignificance in the microstructure variation of AZ31 becomes visible in a very small range for the grain size function and no clear resolvable tendency for the variation of the TYS. The more pronounced broader range for the grain structures of the ZX10 and ZN10 alloys is in comprehensive agreement with a grain size related strengthening mechanism. While the variation of TYS



for ZX10 and ZN10 is somewhat comparable at higher grain sizes (on the left-hand side of the diagram) the variation for both alloys at smallest grain size is significant. Again, this is in agreement with the above discussed fraction of unrecrystallized grains of this condition due to strain hardening. Furthermore, the slightly higher TYS of AZ31 in the respective grain size range in comparison to an interpolated assumption for ZX10 and ZN10 corresponds well to the strong basal textures of this alloy and the resulting limitation of slip activation.

A potential impact of precipitates as strengtheners of the extruded samples as well as their heat treated counterparts would impose a further strengthening mechanism likely to occur at least in ZX10 and ZN10. However, in the context of the solid solution annealing of the lean alloy billets prior to extrusion this effect may not be very significant for the samples of this study (Nie, 2012) and especially not resolved within the complexity of the above mentioned microstructure variations. In a consideration of the ability to design preferred mechanical properties of the alloys of this study, particle strengthening would enable a post-forming adjustment of the material strength, thereby maintaining a preferential formability after extrusion.

In combination, the enhancement of these strengthening mechanisms, orientation strengthening, partly recrystallized

microstructure (and potential precipitation strengthening) counteract to an improved formability of the materials of this study. The same is concluded for a respective grain size strengthening if the corresponding microstructure development results in partly recrystallization, e.g., in the case of ZN10 compared to ZX10 after slow extrusion. Furthermore, the design of textures which lead to preferential forming properties during extrusion is based on partly recrystallized microstructures because the resulting texture needs to be weak. This is accessible if the dynamic recrystallization is retarded in a way that not only a strong recrystallization texture is obtained. Interestingly, the texture development as a result of static recrystallization during heat-treatment differs from the texture development at higher extrusion speed, a result of dynamic recrystallization. This is especially obvious in the case of ZN10. Still, annealing is required to increase the degree of recrystallization of this material, i.e., softening the samples.

## CONCLUSIONS

Direct extrusion of flat bands has been used to study alloying and processing effects on the microstructure and texture development. An increase of the extrusion speed is used to induce deformation heating during extrusion and concurrently enhanced dynamic recrystallization. Besides a comprehensive behavior of increased degree of recrystallization and/or grain growth, significant variations in the texture development are found, ranking from classical strong basal textures for AZ31, strong alignments of basal planes with tilt toward ED for ZX10 and the same for the Nd containing ZN10 alloy if the samples are fully recrystallized. This texture has been associated with the typically weak textures obtained in rare earth or Ca containing round bar extrusions. A distinct texture variation becomes possible if a partly recrystallized microstructure is realized during extrusion which includes a texture component typically not visible in round bar extrusions. During heat treatment, i.e., static recrystallization, this texture component can be maintained.

The mechanical properties in tensile tests and Erichsen cupping tests reveal that for biaxial testing especially weak textures allow increasing the formability. Such weak textures are with no preferred alignment of basal planes parallel to the surface but a tilt out of this orientation. Furthermore, a rotational

symmetry of this tilt around ND increases the formability. Contrary, this is not preferred for uni-axial testing where strong tilt peaks of basal planes lead to increasing ductility. Alloying elements such as Nd in ZN10 allow materials with such textures to be obtained after extrusion. In the case of the Ca containing ZX10, recrystallizations was not restricted enough to pronounce this and in the conventional magnesium alloys like AZ31 no hint for the ability to change the texture has been observed. Thus, retardation of dynamic recrystallization by alloying and adjusting the processing parameters (followed by static recrystallization during heat treatment) allows the extrusion of flat profiles with excellent forming properties. The resulting Erichsen values for flat bands (sheets) of ZX10 (6.1 mm) and ZN10 (7.2 mm) are among the higher levels revealed for magnesium sheets.

## DATA AVAILABILITY STATEMENT

The datasets generated for this study are available on request to the corresponding author.

## AUTHOR CONTRIBUTIONS

Experimental works were carried out by MN and JB with continuous discussion with DL and KK. All authors discussed the experimental results and the conclusion and contributed to writing the submitted manuscript.

## FUNDING

The manuscript includes original work from institutional funding of the Helmholtz-Zentrum Geesthacht. The work was also related to a project proposal funded by the Deutsche Forschungsgemeinschaft. The support under Grant nos. Bo 2461/4-1, Yi 103/3-2 and BR 961/7-1 is highly appreciated.

## ACKNOWLEDGMENTS

The authors would like to thank Mr. Günther Meister and Mr. Alexander Reichart for their help during casting and machining of the billets. We also appreciate the great support of Dr. Sangbong Yi during the EBSD measurements of this study.

## REFERENCES

- Agnew, S. R., Yoo, M. H., and Tomé, C. N. (2001). Application of texture simulation to understanding mechanical behavior of Mg and solid solution alloys containing Li or Y. *Acta Mater.* 49, 4277–4289. doi: 10.1016/S1359-6454(01)00297-X
- Al-Samman, T. (2013). Modification of texture and microstructure of magnesium alloy extrusions by particle-stimulated recrystallization. *Mater. Sci. Eng. A* 560, 561–566. doi: 10.1016/j.msea.2012.09.102
- Al-Samman, T., and Li, X. (2011). Sheet texture modification in magnesium-based alloys by selective rare earth alloying. *Mater. Sci. Eng. A* 528, 3809–3822. doi: 10.1016/j.msea.2011.01.080
- Atwell, D. L., and Barnett, M. R. (2007). Extrusion limits of magnesium alloys. *Metallur. Mater. Trans. A* 38, 3032–3041. doi: 10.1007/s11661-007-9323-2
- Bachmann, F., Hielscher, R., and Schaeben, H. (2010). Texture analysis with MTEX – free and open source software toolbox. *Solid State Phenomena* 160, 63–68. doi: 10.4028/www.scientific.net/SSP.160.63
- Ball, E. A., and Prangnell, P. B. (1994). Tensile-compressive yield asymmetries in high strength wrought magnesium alloys. *Scripta Metallur. Materialia* 31, 111–116. doi: 10.1016/0956-716X(94)90159-7
- Barrett, C. D., Imandoust, A., Oppedal, A. L., Inal, K., Tschopp, M. A., and El Kadiri, H. (2017). Effect of grain boundaries on texture formation during dynamic recrystallization of magnesium alloys. *Acta Mater.* 128, 270–283. doi: 10.1016/j.actamat.2017.01.063
- Basu, I., and Al-Samman, T. (2019). Hierarchical twinning induced texture weakening in lean magnesium alloys. *Front. Mater.* 6:187. doi: 10.3389/fmats.2019.00187

- Beausir, B., Biswas, S., Kim, D. I., Tóth, L. S., and Suwas, S. (2009). Analysis of microstructure and texture evolution in pure magnesium during symmetric and asymmetric rolling. *Acta Mater.* 57, 5061–5077. doi: 10.1016/j.actamat.2009.07.008
- Bohlen, J., Cano, G., Drozdenko, D., Dobron, P., Kainer, K., Gall, S., et al. (2018a). Processing effects on the formability of magnesium alloy sheets. *Metals* 8:147. doi: 10.3390/met8020147
- Bohlen, J., Cano, G., Kurz, G., Kainer, K. U., Letzig, D., Drozdenko, D., et al. (2018b). Profile shape effect on the texture and mechanical properties of extruded rare earth containing magnesium alloys. *Acta Phys. Polonica A* 134, 714–719. doi: 10.12693/APhysPolA.134.714
- Bohlen, J., Nürnberg, M. R., Senn, J. W., Letzig, D., and Agnew, S. R. (2007). The texture and anisotropy of magnesium–zinc–rare earth alloy sheets. *Acta Mater.* 55, 2101–2112. doi: 10.1016/j.actamat.2006.11.013
- Bohlen, J., Schlung, O., Gall, S., Müller, S., and Letzig, D. (2016). “Formability of extruded magnesium alloy sheets with different textures,” in *Magnesium Technology 2016*, eds A. Singh, K. Solanki, M. V. Manuel, and N. R. Neelameggham (Hoboken, NJ: John Wiley & Sons, Inc.), 251–256.
- Bohlen, J., Wendt, J., Nienaber, M., Kainer, K. U., Stutz, L., and Letzig, D. (2015). Calcium and zirconium as texture modifiers during rolling and annealing of magnesium–zinc alloys. *Mater. Character.* 101, 144–152. doi: 10.1016/j.matchar.2015.02.002
- Bohlen, J., Yi, S., Letzig, D., and Kainer, K. U. (2010). Effect of rare earth elements on the microstructure and texture development in magnesium–manganese alloys during extrusion. *Mater. Sci. Eng. A* 527, 7092–7098. doi: 10.1016/j.msea.2010.07.081
- Brokmeier, H.-G. (2018). Hot rectangular extrusion textures of six Mg-alloys via neutron diffraction. *Adv. Eng. Mater.* 20:1700234. doi: 10.1002/adem.201700234
- Chapuis, A., and Driver, J. H. (2011). Temperature dependency of slip and twinning in plane strain compressed magnesium single crystals. *Acta Mater.* 59, 1986–1994. doi: 10.1016/j.actamat.2010.11.064
- Chaudry, U. M., Kim, T. H., Park, S. D., Kim, Y. S., Hamad, K., and Kim, J.-G. (2019). Effects of calcium on the activity of slip systems in AZ31 magnesium alloy. *Mater. Sci. Eng. A* 739, 289–294. doi: 10.1016/j.msea.2018.10.060
- Chino, Y., Sassa, K., and Mabuchi, M. (2009). Texture and stretch formability of a rolled Mg–Zn alloy containing dilute content of Y. *Mater. Sci. Eng. A* 513–514, 394–400. doi: 10.1016/j.msea.2009.01.074
- Dillamore, I. L., and Roberts, W. T. (1965). Preferred Orientation in Wrought and Annealed Metals. *Metallur. Rev.* 10, 271–380. doi: 10.1179/mtr.1965.10.1.271
- Elsayed, F. R., Hort, N., Salgado Ordorica, M. A., and Kainer, K. U. (2011). Magnesium permanent mold castings optimization. *Mater. Sci. Forum* 690, 65–68. doi: 10.4028/www.scientific.net/MSF.690.65
- Friedrich, H. E., and Mordike, B. L. (2006). *Magnesium Technology: Metallurgy, Design Data, Applications*. Heidelberg: Springer-Verlag.
- Gall, S., Coelho, R. S., Müller, S., and Reimers, W. (2013). Mechanical properties and forming behavior of extruded AZ31 and ME21 magnesium alloy sheets. *Mater. Sci. Eng. A* 579, 180–187. doi: 10.1016/j.msea.2013.05.027
- Hadorn, J. P., Hantzsche, K., Yi, S., Bohlen, J., Letzig, D., Wollmershauser, J. A., et al. (2011). Role of solute in the texture modification during hot deformation of Mg–rare earth alloys. *Metallur. Mater. Trans. A* 43, 1347–1362. doi: 10.1007/s11661-011-0923-5
- Hantzsche, K., Bohlen, J., Wendt, J., Kainer, K. U., Yi, S. B., and Letzig, D. (2010). Effect of rare earth additions on microstructure and texture development of magnesium alloy sheets. *Scr. Mater.* 63, 725–730. doi: 10.1016/j.scriptamat.2009.12.033
- Hsiang, S.-H., and Kuo, J.-L. (2003). An investigation on the hot extrusion process of magnesium alloy sheet. *J. Mater. Process. Technol.* 140, 6–12. doi: 10.1016/S0924-0136(03)00693-9
- Huang, X., Suzuki, K., Chino, Y., and Mabuchi, M. (2012). Influence of initial texture on rolling and annealing textures of Mg–3Al–1Zn alloy sheets processed by high temperature rolling. *J. Alloys Compd.* 537, 80–86. doi: 10.1016/j.jallcom.2012.05.002
- Jiang, M. G., Xu, C., Nakata, T., Yan, H., Chen, R. S., and Kamado, S. (2016). Development of dilute Mg–Zn–Ca–Mn alloy with high performance via extrusion. *J. Alloys Compd.* 668, 13–21. doi: 10.1016/j.jallcom.2016.01.195
- Kim, S.-J., Lee, Y.-S., and Kim, D. (2016). Analysis of formability of Ca-added magnesium alloy sheets at low temperatures. *Mater. Character.* 113, 152–159. doi: 10.1016/j.matchar.2016.01.013
- Kree, V., Bohlen, J., Letzig, D., and Kainer, K. U. (2004). The metallographical examination of magnesium alloys. *Pract. Metallogr.* 41, 233–246.
- Lee, J.-Y., Yun, Y.-S., Suh, B.-C., Kim, N.-J., Kim, W.-T., and Kim, D.-H. (2014). Comparison of static recrystallization behavior in hot rolled Mg–3Al–1Zn and Mg–3Zn–0.5Ca sheets. *J. Alloys Compd.* 589, 240–246. doi: 10.1016/j.jallcom.2013.11.210
- Liu, G., Zhou, J., and Duszczek, J. (2007). Prediction and verification of temperature evolution as a function of ram speed during the extrusion of AZ31 alloy into a rectangular section. *J. Mater. Process. Technol.* 186, 191–199. doi: 10.1016/j.jmatprotec.2006.12.033
- Liu, L., Pan, F., Chen, X., Huang, Y., Song, B., Yang, H., et al. (2018). The effect of Y addition on recrystallization and mechanical properties of Mg–6Zn–xY–0.5Ce–0.4Zr alloys. *Vacuum* 155, 445–455. doi: 10.1016/j.vacuum.2018.06.048
- Liu, P., Jiang, H., Cai, Z., Kang, Q., and Zhang, Y. (2016). The effect of Y, Ce and Gd on texture, recrystallization and mechanical property of Mg–Zn alloys. *J. Magnes. Alloys* 4, 188–196. doi: 10.1016/j.jma.2016.07.001
- Liu, Y., Li, N., Arul Kumar, M., Pathak, S., Wang, J., McCabe, R. J., et al. (2017). Experimentally quantifying critical stresses associated with basal slip and twinning in magnesium using micropillars. *Acta Mater.* 135, 411–421. doi: 10.1016/j.actamat.2017.06.008
- Mann, G., Griffiths, J. R., and Cáceres, C. H. (2004). Hall-Petch parameters in tension and compression in cast Mg–2Zn alloys. *J. Alloys Compd.* 378, 188–191. doi: 10.1016/j.jallcom.2003.12.052
- Miller, V. M., Berman, T. D., Beyerlein, I. J., Jones, J. W., and Pollock, T. M. (2016). Prediction of the plastic anisotropy of magnesium alloys with synthetic textures and implications for the effect of texture on formability. *Mater. Sci. Eng. A* 675, 345–360. doi: 10.1016/j.msea.2016.08.063
- Minárik, P., Drozdenko, D., Zemková, M., Veselý, J., Capek, J., Bohlen, J., et al. (2019). Advanced analysis of the deformation mechanisms in extruded magnesium alloys containing neodymium or yttrium. *Mater. Sci. Eng. A* 759, 455–464. doi: 10.1016/j.msea.2019.05.069
- Mordike, B. L., and Ebert, T. (2001). Magnesium properties - applications - potential. *Mater. Sci. Eng. A* 302, 37–45. doi: 10.1016/S0921-5093(00)01351-4
- Nascimento, L., Yi, S., Bohlen, J., Fuskova, L., Letzig, D., and Kainer, K. U. (2010). High cycle fatigue behaviour of magnesium alloys. *Procedia Eng.* 2, 743–750. doi: 10.1016/j.proeng.2010.03.080
- Nie, J.-F. (2012). Precipitation and hardening in magnesium alloys. *Metall. Mater. Trans. A* 43, 3891–3939. doi: 10.1007/s11661-012-1217-2
- Stanford, N. (2010a). The effect of calcium on the texture, microstructure and mechanical properties of extruded Mg–Mn–Ca alloys. *Mater. Sci. Eng. A* 528, 314–322. doi: 10.1016/j.msea.2010.08.097
- Stanford, N. (2010b). Micro-alloying Mg with Y, Ce, Gd and La for texture modification—a comparative study. *Mater. Sci. Eng. A* 527, 2669–2677. doi: 10.1016/j.msea.2009.12.036
- Stanford, N. (2013). The effect of rare earth elements on the behaviour of magnesium-based alloys: part 2 – recrystallisation and texture development. *Mater. Sci. Eng. A* 565, 469–475. doi: 10.1016/j.msea.2012.10.084
- Stanford, N., and Barnett, M. (2008a). Effect of composition on the texture and deformation behaviour of wrought Mg alloys. *Scripta Materialia* 58, 179–182. doi: 10.1016/j.scriptamat.2007.09.054
- Stanford, N., and Barnett, M. R. (2008b). The origin of “rare earth” texture development in extruded Mg-based alloys and its effect on tensile ductility. *Mater. Sci. Eng. A* 496, 399–408. doi: 10.1016/j.msea.2008.05.045
- Stutz, L., Bohlen, J., Letzig, D., and Kainer, K. U. (2011). “Formability of Magnesium sheet ZE10 and AZ31 with respect to initial texture,” in *Magnesium Technology 2011*, eds W. H. Sillekens, S. R. Agnew, N. R. Neelameggham, and S. N. Mathaudhu (Hoboken, NJ: John Wiley & Sons, Inc.), 373–378.
- Styczynski, A., Hartig, C., Bohlen, J., and Letzig, D. (2004). Cold rolling textures in AZ31 wrought magnesium alloy. *Scripta Materialia* 50, 943–947. doi: 10.1016/j.scriptamat.2004.01.010
- Suh, J., Victoria-Hernandez, J., Letzig, D., Golle, R., Yi, S., Bohlen, J., et al. (2015). Improvement in cold formability of AZ31 magnesium alloy sheets processed by equal channel angular pressing. *J. Mater. Process. Technol.* 217, 286–293. doi: 10.1016/j.jmatprotec.2014.11.029

- Victoria-Hernandez, J., Yi, S., Bohlen, J., Kurz, G., and Letzig, D. (2014). The influence of the recrystallization mechanisms and grain growth on the texture of a hot rolled AZ31 sheet during subsequent isochronal annealing. *J. Alloys Compounds* 616, 189–197. doi: 10.1016/j.jallcom.2014.07.083
- Wang, H., Wu, P. D., Boyle, K. P., and Neale, K. W. (2011). On crystal plasticity formability analysis for magnesium alloy sheets. *Int. J. Solids Struct.* 48, 1000–1010. doi: 10.1016/j.ijsolstr.2010.12.004
- Wang, Q., Jiang, B., Chai, Y., Liu, B., Ma, S., Xu, J., et al. (2016). Tailoring the textures and mechanical properties of AZ31 alloy sheets using asymmetric composite extrusion. *Mater. Sci. Eng. A* 673, 606–615. doi: 10.1016/j.msea.2016.07.111
- Wang, W., Ma, L., Chai, S., Zhang, W., and Feng, Y. (2018). Role of one direction strong texture in stretch formability for ZK60 magnesium alloy sheet. *Mater. Sci. Eng. A* 730, 162–167. doi: 10.1016/j.msea.2018.05.113
- Yi, S., Brokmeier, H.-G., and Letzig, D. (2010). Microstructural evolution during the annealing of an extruded AZ31 magnesium alloy. *J. Alloys Compounds* 506, 364–371. doi: 10.1016/j.jallcom.2010.07.008
- Yi, S., Davies, C. H. J., Brokmeier, H. G., Bolmaro, R. E., Kainer, K. U., and Homeyer, J. (2006). Deformation and texture evolution in AZ31 magnesium alloy during uniaxial loading. *Acta Materialia* 54, 549–562. doi: 10.1016/j.actamat.2005.09.024
- Yu, H., Hyuk Park, S., Sun You, B., Min Kim, Y., Shun Yu, H., and Soo Park, S. (2013). Effects of extrusion speed on the microstructure and mechanical properties of ZK60 alloys with and without 1 wt% cerium addition. *Mater. Sci. Eng. A* 583, 25–35. doi: 10.1016/j.msea.2013.06.073
- Zeng, X., Minárik, P., Dobron, P., Letzig, D., Kainer, K. U., and Yi, S. (2019). Role of deformation mechanisms and grain growth in microstructure evolution during recrystallization of Mg-Nd based alloys. *Scripta Materialia* 166, 53–57. doi: 10.1016/j.scriptamat.2019.02.045
- Zhou, N., Zhang, Z., Dong, J., Jin, L., and Ding, W. (2013). High ductility of a Mg–Y–Ca alloy via extrusion. *Mater. Sci. Eng. A* 560, 103–110. doi: 10.1016/j.msea.2012.09.042

**Conflict of Interest:** The authors declare that the research was conducted in the absence of any commercial or financial relationships that could be construed as a potential conflict of interest.

Copyright © 2019 Nienaber, Kainer, Letzig and Bohlen. This is an open-access article distributed under the terms of the Creative Commons Attribution License (CC BY). The use, distribution or reproduction in other forums is permitted, provided the original author(s) and the copyright owner(s) are credited and that the original publication in this journal is cited, in accordance with accepted academic practice. No use, distribution or reproduction is permitted which does not comply with these terms.